Proceedings of the ASME 2022 International Technical Conference and Exhibition on
Packaging and Integration of Electronic and Photonic Microsystems
InterPACK2022
October 24-28, 2022, Anaheim, California

IPACK2022- 97400

EXPERIMENTAL INVESTIGATION OF R134A FLOW BOILING IN COPPER FOAM EVAPORATORS FOR HIGH HEAT FLUX ELECTRONICS COOLING

*D. Kisitu[1], C. Caceres[1], M. Zlatinov[2], D. Schaffarzick[2], A. Ortega[1]

[1]Laboratory for Advanced Thermal and Fluid Systems (LATFS)
NSF – Center for Energy-Smart Electronic Systems (ES2)
Villanova University, Villanova, PA 19085, USA
*dkisitu@villanova.edu

[2]ERG Aerospace Corporation
964 Stanford Ave, Oakland, CA 94608, USA

ABSTRACT

Stochastic cellular structured materials have been previously studied as enhanced surfaces for heat sinks used in cooling of modern electronics. Open-cell metallic foam has been shown to be an effective medium for gas-cooled and liquid-cooled heat sinks. Numerous studies exist for metal-foam cold plates using single phase water but there are few studies pertinent to two-phase evaporators. Because of the latent heat of vaporization and higher heat transfer coefficients, flow boiling is more efficient for cooling of high heat fluxes, as compared to single-phase flow. This paper presents an experimental study on the thermohydraulic performance of compressed and uncompressed copper foam evaporators using R134a refrigerant. The foam samples had the same starting pore size of 40 PPI and porosities of 0.62-0.91, with a heated footprint area of 25.4x25.4 mm and a height of 2.5 mm. Experiments were conducted for heat flux ranging from 7 to 174 W/cm^2, with mass flux varying from 150 to 375 kg/m^{2}s at fixed inlet saturation temperatures of 31 to 33 ^{o}C. Compressing the foam by up to 4X resulted in proportionally smaller effective hydraulic diameter, higher surface area per unit volume, higher metal volume fraction, and higher bulk thermal conductivity. The compressed foam results demonstrated up to three-times lower unit thermal resistance and improved critical heat flux. The apparent heat transfer coefficient in the tested compressed 4X foam evaporator maximized at exit vapor qualities of about 70 to 75 %, and the pressure drop increased linearly with exit quality.

Keywords: Metallic foam, Compressed foam, Flow boiling, Porous media, Electronics cooling, High heat flux, Two phase cooling

NOMENCLATURE

A	Area, m^2
c_p	Specific heat, $J/kg \cdot K$
CR	Compression ratio
CHF	Critical Heat Flux, W/m^2
G	Effective mass flux, $kg/m^2 \cdot s$
h	Heat transfer coefficient, $W/m^2 \cdot K$
h'	Specific enthalpy, J/kg
I	Current, A
k	Thermal conductivity, $W/m \cdot K$
L	Base plate length, m
$\dot{m}$	Mass flow rate, kg/s
P	Pressure, Pa
PPI	Pores Per Inch
PCM	Phase Change Material
Q	Power, W
q''	Heat flux, W/m^2
R''	Unit thermal resistance, $K \cdot m^2/W$
t	Thickness, m
T	Temperature, K
TIM	Thermal Interface Material
V	Voltage, V
W	Width, m
x	Vapor quality
X	Streamwise direction
Y	Vertical direction
Z	Spanwise direction

Greek Symbols

ΔP	Pressure drop, Pa
$\Delta P/L$	Pressure drop per unit length, Pa/m
ΔT	Temperature difference, K
ε	Porosity ($Void\ space\ volume/Bulk\ volume$)

Subscripts

act	Actual
app	Apparent
base	Base
Cu	Copper
ele	Electrical
f	Liquid phase
fm	Foam
g	Vapor phase
in	Inlet
i	Direction *i*
j	Direction orthogonal to *i*
k	Direction orthogonal to *i* and *j*
loss	Losses
mean	Mean
out	Outlet/Exit
sat	Saturation
unit	Unit
wall	Wall

1. INTRODUCTION

Heat dissipation is one of the most critical issues for the reliability of electronics [1]. The advent of high-performance electronics is steadily increasing the heat fluxes to be managed [2]. Efficient, innovative thermal management solutions are therefore needed to maintain allowable junction temperatures, especially using compact heat sinks which can be either two-phase cooled [3]–[6] or single-phase liquid-cooled [2], [7]. Heat transfer enhancement using porous media such as metal foams are being considered as alternatives to manufactured fin structures for electronics cooling. Open-cell metal foams consist of a network of interconnected ligaments, forming a porous metal structure with good thermal conductivity, high surface area to volume ratio, and attractive stiffness and strength [8]. Heat transfer is further augmented due to the boundary layer restart and enhanced mixing effects of the stochastic ligament structure. To date, most of the heat transfer studies have focused on single-phase thermohydraulic performance of metal foams, with few investigations on two-phase flow and heat transfer in these tortuous materials. Although two-phase flow in microchannels has been extensively investigated due to its high thermal performance, Kandlikar et al. [6] reported major issues hindering its practical application, among which include flow instability and low CHF. Metallic foams [9] are promising alternatives to machined microchannels [4]–[6], [10] for indirect two-phase cold plates or evaporators used in high heat flux electronics cooling as this porous media may mitigate some of the issues arising in parallel microchannels.

There have been relatively few investigations on two-phase flow in metal foams. Flow boiling characteristics of three copper foams, including 0.95 porosity and 10 PPI, 0.95 porosity and 20 PPI, and 0.92 porosity and 20 PPI, were experimentally studied by Kim et al. [11]. Mass fluxes from 20 to 72 kg/m^{2}s and heat fluxes of about 6 to 27 W/cm^2 were tested. Results revealed that the foam sample with high porosity and large pore size (0.95 porosity and 10 PPI) gave the best thermal performance, attaining a heat transfer coefficient of 10 kW/m^2 K. They concluded that foam porosity can have a slight effect of up to 23%, on the heat transfer coefficient at high heat fluxes, and for a fixed porosity, larger pore size gave higher enhancement on heat transfer.

Pranoto and Leong [12] investigated flow boiling, using FC-12, in evaporators with graphite porous foams with porosities of 0.61 and 0.72, and with bypass gaps of 6, 4, and 2 mm. Mass fluxes of 50, 100, and 150 kg/m^{2}s and heat fluxes of 4 to 83.3 W/cm^2 were investigated. The results showed that using of graphite foams of 0.61 and 0.72 porosities augmented the heat transfer coefficients by up to 2.5 and 1.9 times, compared to a bare surface. A maximum local heat transfer coefficient of 16.5 kW/m^2 K was achieved with 0.61-porosity foam at a mass flux of 150 kg/m^{2}s and a gap of 6 mm gap. From their high-speed visualization, more bubble departure frequency was observed from the 0.61-porosity foam, attributed to more active nucleation sites, which led to a higher thermal performance augmentation.

In another study, using Selective Laser Melting (SLM), an additive manufacturing technique, Wong and Leong [13] fabricated specialized 3D porous metallic structures. Flow boiling experimental study was performed using FC-72 refrigerant, and sphere-small (0.36 porosity), sphere-large (0.72 porosity) and gradient reverse or forward (0.54 porosity) porous metallic samples were tested, with mass fluxes ranging from 20 to 400 kg/m^{2}s and heat fluxes of 1 to 16 W/cm^2. The porous samples enhanced flow boiling heat transfer due to increased nucleation sites and intensified flow mixing. The gradient reverse porous substrate had the highest heat transfer enhancement, attributed to the channeling of the liquid-vapor mixture into tinier cross-sectional areas and delaying of dry out for high vapor quality. It was concluded that for any subject porous sample type, the heat transfer coefficient rises as the exit vapor quality increases and maximizes at exit qualities of about 30 to 60 %, beyond which it degrades.

Using a vertical orientation, Madani et al. [1] investigated flow boiling inside a channel filled with 36 PPI and 0.97-porosity copper foam using n-pentane. Mass fluxes ranging from 10 to 100 kg/m^{2}s and heat fluxes from 0 to 25 W/cm^2 were tested. Their comparison with the Gungore-Winterton correlation [14] revealed that the metallic foam insert increases the heat transfer coefficient up to 4-fold, at low quality.

Mancin et al. [15] experimentally compared thermohydraulic performance of R134a and R1234ze(E) with single-phase and flow boiling in a 5 PPI copper foam. Heat fluxes of 5 and 10 W/cm^2 and mass fluxes of between 50 to 200 kg/m^{2}s were test at a fixed saturation temperature of 30 ºC. It was revealed that thermohydraulic performance of R134a is better than that obtained from R1234ze. The higher pressure drops associated with R1234ze was attributed to its higher liquid-vapor density ratio that induced higher shear stress. Diani et al. [8] extended the experimental investigation using in the same test setup in [15]. Heat transfer performance of R1234yf, R1234ze(E) and R134a were tested during flow boiling. Results show that, for all refrigerants, the pressure drops increase linearly with both vapor quality and mass flux and R1234ze(E) had the highest pressure drops, especially at high mass flux. They revealed that heat transfer coefficients could be increased up to 4.8 times, compared to the prediction of the Gungor-Winterton correlation [14]. It was shown that R134a has the best thermal performance, followed by R1234yf.

Conventionally, flow boiling heat transfer in small channels is mainly governed by nucleate boiling and convective boiling mechanisms. In channels, convective boiling results from the convective effects with dominance at high mass fluxes, while nucleate boiling results from the nucleating bubbles and their subsequent growth and departure at the heated surface, with dominance at low Reynold numbers [16]. Thin film evaporation is also reported to be an additional mechanism in smaller cross sectional microchannels due to bubble confinement effects [10]. Inadequate investigations on flow boiling mechanisms in metallic foam exist in the literature.

The current study is motivated by the clear lack of quality experimental data for two-phase heat transfer with refrigerants in metallic foams for heat fluxes greater than 100 W/cm^2. Modern electronics cooling requires managing heat fluxes up to 200 W/cm^2 or higher. Secondly, previous preliminary work by this team on single-phase water cooling has shown that selective foam compression leads to dramatic increase in thermal performance. Thus, the current work is an initial investigation to determine if foam compression has similar benefits in two-phase refrigerant cooling. This work focuses on experimentally investigating the effect of metal foam compression on thermohydraulic performance, with heat fluxes up to 174 W/cm^2 using R134a as a working fluid. Data are presented for copper foams with up to 4X compression. The aggregate data reveal that compression leads to major improvement in the thermal performance and boiling trends that are quite different from flow boiling in traditional microchannels.

2. Experimental Setup and Test Procedure

2.1 Experimental Setup

The experimental rig, illustrated in Figure 1, was designed to control and measure the test section inlet conditions. The two-phase flow loop is divided in three sections the test section, the condenser section, and the flow conditioning section. Upstream of the test section is the brazed plate heat exchanger condenser, where heat rejection is achieved by a NESLABTM HX Series recirculating chiller that controls the condensation temperature. The saturated liquid refrigerant is stored in the reservoir instrumented with a 1/8 in type-K thermocouple probe and a 0-300 psi Omega^{TM} PX209 pressure transducer. The reservoir achieves saturation conditions and therefore equilibrates to its saturation pressure at the reservoir temperature. The liquid refrigerant from the base of the tank is pumped by a positive displacement gear pump with a digital speed controller. The flow leaving the pump is filtered and then metered by an Emerson^{TM} Micro Motion® ELITE® Coriolis flowmeter. Finally, the flow temperature is precisely controlled by passing the flow through a coiled-tube heat exchanger immersed in a ThermoNESLAB isothermal bath which allows precise control of the temperature and therefore the degree of subcooling entering the evaporator.

The evaporator inlet temperature and pressure are measured using an inline 1/8 in type-K thermocouple probe and a 0-300 psi Omega^{TM} PX209 pressure transducer. The average evaporator base temperature is measured with a butt-welded type-K thermocouple embedded in the center of the evaporator base. The pressure drop across the evaporator is directly measured using a 0-50psid Setra^{TM} DPT2301 differential pressure transducer. The temperature of the two-phase mixture exiting the evaporator is measured by an inline 1/8 in type-K thermocouple probe.

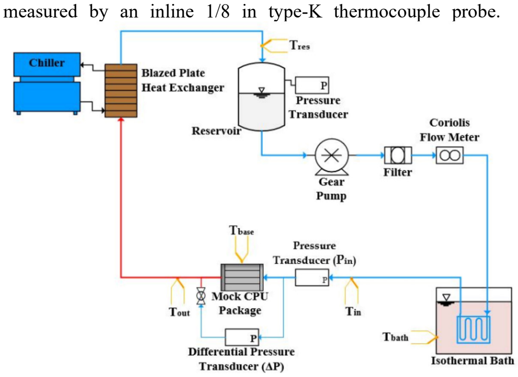

Figure 1: Schematic of two-phase setup

2.2 Test Section

The test section, shown in Figure 2 (a), is comprised of a base with a seat for the test article and a lid with a transparent viewing window. Both the base and the lid are fabricated from stainless steel. The base is designed so as to allow flow to enter the inlet manifold from below and exit through the outlet manifold through flow ports that match the ports in the manifolds of the test article, Figure 2 (c). Heat is supplied to the 1 in. x 1 in. base of the test article by a heat concentrator bar with a 1 in. x 1 in. cross-section. The test section is mounted onto the surface of the bar with a spring-loaded hold-down fixture. The spring loading allows precise and repeatable control of the loading pressure, set to about 29 psi. A Honeywell PTM 7950 PCM TIM with thermal conductivity of about 8.5 W/m-K, was used between the evaporator base and the concentrator. The heat concentrator, Figure 2 (b), is made of copper with an upper rod, 1 in. x 1 in. in cross-section transitioning to a large base with four embedded Tempco cartridge heaters. The four heaters are connected in parallel to a KEYSIGHT N8762A DC Power Supply. The concentrator allows direct measurement of the temperature gradient through the bar using four equally spaced type-K thermocouples embedded to the bar centerline. Fourier's law is used to determine the heat flow using the known thermal conductivity of the copper rod.

2.3 Foam Test Samples

The test coupons consisted of a copper base with a machined pocket allowing the foam sample to sit in the middle with a well-defined flow manifold at the inlet and exit as seen in Figure 3. The foam samples measured 25.4 x 25.4 mm x 2.5 mm. The base was 2 mm thick. ERG Duocel® copper foam test samples [9] were soldered onto the base in an inert environment using SAC 305 (96.5% Sn, 3% Ag, and 0.5% Cu) solder foil. Figure 3 shows the two test coupons used in this study – one with uncompressed foam, and one with foam compressed by a factor of 4X, i.e., ratio of the initial volume to final volume of the sample is 4. It is important to note that the direction of the compression was in the streamwise direction, i.e., in the x-direction shown in Fig. 3. Table 1 shows details about the foam samples and their structure. The surface area estimates are based on CT-scan data collected by ERG Aerospace on comparable 40 PPI metal foams. Compressing the metal foam increases the surface area per unit volume proportionally. Foam sample B was deliberately compressed in the streamwise direction to increase foam effective thermal conductivity in the y-direction, i.e., in the direction of the applied heat flux while also minimizing pressure drop impact due to compression.

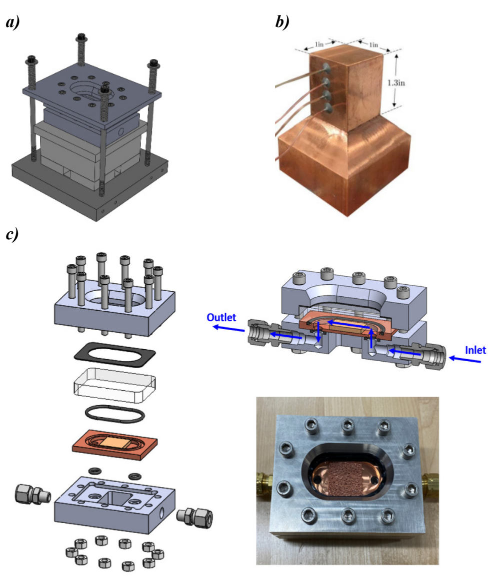

Figure 2: (a) Test section loading assembly, (b) Concentrator, and (c) Test section assembly with exploded view and flow configuration

Thermal conductivity is estimated based on Eqn. (1), and is a function of the porosity, the conductivity of the metal, and the compression ratios (*CR*) parallel and orthogonal to each dimension.

$$k_{fm,i} = \frac{1}{3}\left(1-\varepsilon_{fm}\right)\cdot k_{Cu}\frac{CR_j.CR_k}{CR_i} \tag{1}$$

The factor of 1/3 was shown by Krishnan et al. [17] to closely match empirical data for thermal conductivity of open-celled metal foams. Ozmat et al. [18] demonstrated the importance of compression direction on the effective conductivity of compressed foam – namely that thermal conductivity increases proportionally to compression ratio in the direction orthogonal to compression but decreases proportionally in the direction parallel to compression. Compressing in the streamwise direction also has the additional benefit of keeping the pores open to the incoming flow, resulting in a comparatively lower pressure drop penalty derived from compression.

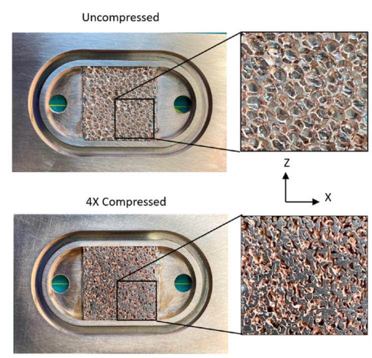

Figure 3: Uncompressed and compressed (4X) test coupons

2.4 Test procedure

All experiments were conducted using R134a as the working fluid. To investigate the effect of compression, identical tests were conducted on uncompressed (sample A) and 4X-compressed (sample B) Cu foams [9], with details given in Table 1. For the initial tests shown in Figures 4 and 5, the inlet saturation temperature and degree of subcooling were held constant at 33 ºC and 3 ºC respectively. Mass flow rate was held constant at 15 g/s. Heat flux was varied from 7 to 103 W/cm^2.

For only 4X compressed sample, other tests were performed to study the effects of mass flux, heat flux, and exit vapor quality while holding constant the saturation temperature to 31 ºC and degree of subcooling to 1 ºC. Mass flux was varied from 150 kg/m^{2}s (6 g/s) to 250 kg/m^{2}s (10 g/s), heat flux was varied from 7 to 174 W/cm^2 and exit vapor quality varied from 3 to 100%.

The thermophysical properties of R134a were obtained from CoolProp [19].

Table 1: Foam characteristics provided by ERG Aerospace [9]

	Foam Sample	A	B
Coupon	Foam Length (L_{fm}) [mm]	25.4	25.4
	Foam Width (W_{fm}) [mm]	25.4	25.4
	Foam Thickness (t_{fm}) [mm]	2.5	2.5
	Base Area (A_{base}) [cm^2]	6.45	6.45
	Base Thickness [mm]	2.0	2.0
Foam	PPI	40	40
	Nominal Compression Ratio (CR)	-	4
	Compress Direction	-	X
	Initial Porosity	0.91	0.90
	Final Porosity	0.91	0.62
	Effective Compression Ratio (CR)	1.00	3.85
	Surface Area per Unit Volume [m^2/m^3]	910	3560
Thermal Conductivity	Foam Material	C10100	C10100
	k_{Cu} [W/m-K]	390	390
	$k_{fm,X}$ [W/m-K]	12.0	3.3
	$k_{fm,Y}$ [W/m-K] (heat flux direction)	12.0	49.5
	$k_{fm,Z}$ [W/m-K]	12.0	49.5

2.5 Data Reduction

The electrical power, Q_{ele} supplied by the cartridge heaters in the concentrator base, was obtained from the product of voltage, V and current, I ;

$$Q_{ele} = I \cdot V \tag{2}$$

The applied heat flux, q'' was determined, as described in [5], using Fourier's law for 1-D steady-state conduction on the temperatures measured from four equally spaced thermocouples installed in the heat concentrator.

$$q'' = -k_{Cu}\frac{dT}{dx} \tag{3}$$

The actual power input, Q_{act} is obtained from the product of heat flux, q'' and the concentrator top footprint area, which is equal to the evaporator base area, A_{base} , in the current setup:

$$Q_{act} = q'' \cdot A_{base} \tag{4}$$

The power losses were determined from Eqn. (5):

$$Q_{loss} = Q_{ele} - Q_{act} \tag{5}$$

The exit vapor quality of the test section is defined as:

$$x_{out} = \frac{h'_{out} - h'_f}{h'_g - h'_f} \tag{6}$$

Where, the exit specific enthalpy of the test section, h'_{out} can be computed from the energy balance applied to the test section:

$$h'_{out} = h'_{in} + \frac{Q_{act}}{\dot{m}} \tag{7}$$

The inlet specific enthalpy is evaluated from the inlet pressure and refrigerant temperature.

$$h'_{in} = h'\left(P_{in}, T_{in}\right) \tag{8}$$

The fluid and gas specific enthalpies, h'_f and h'_g , are computed at the outlet saturation pressure of the test section.

$$h'_f = h'\left(P_{sat,out}\right) \tag{9}$$

$$h'_g = h'\left(P_{sat,out}\right) \tag{10}$$

The two-phase apparent heat transfer coefficient, based on the base footprint area, A_{base} , is defined as [8], [15]:

$$h_{app} = \frac{Q_{act}}{A_{base}\left(T_{sat,mean} - T_{wall}\right)} \tag{11}$$

Where the mean saturation temperature is defined as the average of outlet and inlet saturation temperatures [8], [15]:

$$T_{sat,mean} = \frac{\left(T_{sat,in} + T_{sat,out}\right)}{2} \tag{12}$$

The unit thermal resistance for the evaporator is defined as

$$R'' = \frac{\left(T_{base} - T_{in}\right)}{q''} \tag{13}$$

The effective mass flux through the metal foam open cross-section is defined in Eqn. (14).

$$G = \frac{\dot{m}}{\varepsilon_{fm} \cdot W \cdot t} \tag{14}$$

The pressure drop per unit length through the metal foam can be computed from:

$$\Delta P / L = \frac{\Delta P_{fm}}{L_{fm}} \tag{15}$$

3. RESULTS AND DISCUSSION

3.1 Effect of compression on thermohydraulic performance

The unit thermal resistance derived from uncompressed (A) and compressed foam (B) are plotted as a function of heat flux, at a constant mass flow rate, $\dot{m}$ of 15 g/s, with inlet saturation temperature and subcooling of 33ºC and 3ºC, respectively. Figure 4. The foam compression reduces the unit thermal resistance by up to about 300%. This is attributed to the higher surface area per unit volume and higher bulk thermal conductivity in the heat flux direction, both of which increase proportionally with compression ratio, as noted in Table 1. We also postulate that the smaller effective pores in compressed foam may introduce bubble confinement effects, which may result in thin-film evaporation as a dominant heat transfer phenomenon. Similar observations have been previously made in flow boiling in smaller cross-section microchannels [10]. Remarkably, the thermal resistance for the compressed foam is largely independent of heat flux for these test conditions. By comparison, the thermal resistance of the uncompressed foam strongly decreased with heat flux up to 45 W/cm^2 and then showed similar insensitivity to heat flux as the compressed sample. By inference to documented flow boiling behavior in small channels it may be that insensitivity to heat flux indicates convective boiling dominance, whereas the strong dependence on heat flux may be due to dominance of nucleate boiling, although such comparisons do not account for the tortuous flow pathways that are unique to the open foam structure.

For the aforementioned test conditions, Figure 5 shows the pressure drop trends for the two foam samples as a function of heat flux. As expected, the higher thermal performance of the compressed foam is accompanied by a higher pressure drop. This is because, as shown in Table 1, compressing the foam significantly decreases the hydraulic diameter, which generates more flow impedance for a fixed mass flow rate, compared to the uncompressed foam. For the presently tested configurations, the additional pressure drop penalty for compressed foam is commensurate to the thermal performance advantage, i.e., the pressure drop increases by 300% while the thermal resistance decreases by 300%.

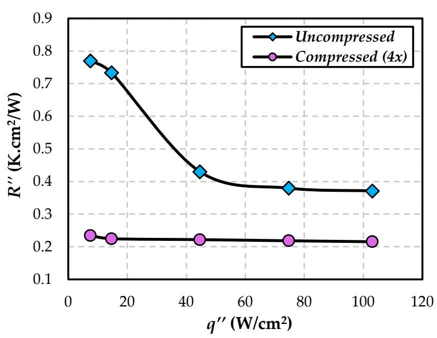

Figure 4: Comparison of thermal resistance for uncompressed and compressed 4X foams

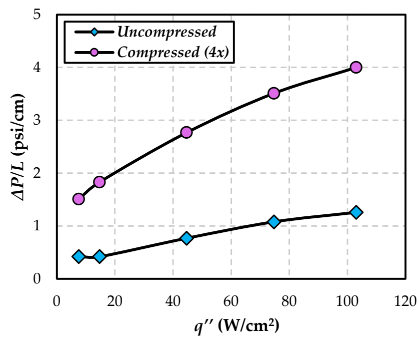

Figure 5: Comparison of pressure drop for uncompressed and compressed 4X foams

3.2 Effect of mass flux and exit vapor quality on compressed foam performance

3.2.1 Flow boiling curves

The 4X compressed foam was tested at different mass flux conditions. For three mass fluxes, the heat flux as a function of wall superheat are plotted in Figure 6. The boiling curves initially collapse to a single curve and the wall superheat increases with heat flux, which most likely indicates dominance of nucleate boiling. At higher heat flux, a dependence on mass flux is observed as the behaviors diverge for differing mass flux.

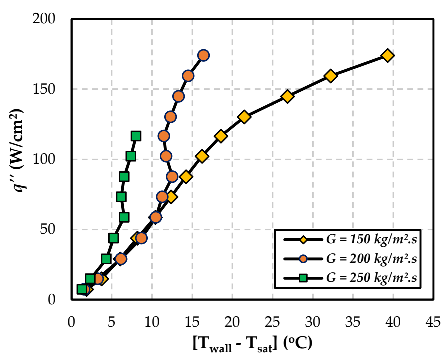

Figure 6: Boiling curves at different mass fluxes

At the higher mass fluxes of 200 and 250 kg/m^{2}s, the wall superheat is mostly independent of heat flux at high heat flux, which may indicate dominance of convective boiling at both high mass flux and heat flux. It should be noted here that the limits of the achievable heat flux for the three mass flow rates was determined by the pressure drop and the ability of the rig pump to overcome the increasing pressure drop at high mass flow rate and high vapor quality. Thus, at the two highest flow rates, there is no indication of onset of dryout or critical heat flux, but no doubt this will be observed at increasing heat flux just as it is at the smallest mass flux tested

For the lowest mass flux (150 kg/m^{2}s), the boiling curve does exhibit an inflection point beyond a heat flux of 130 W/cm^2, an initial indication of the onset of dry-out conditions at high vapor quality.

3.2.2 Apparent Heat Transfer Coefficient and Unit Thermal Resistance

The apparent heat transfer coefficients are plotted as a function of heat flux in Figure 7. At the lowest heat flux, even with low subcooling, it is expected that the heat transfer is in the single-phase regime and hence is dependent only on mass flow rate. This is confirmed by the data. At increasing heat flux, after the onset of nucleate boiling, the data for all mass fluxes are consistent and appear to show at least three regimes or behaviors. First, the heat transfer coefficient increases with a moderate dependence on heat flux, followed by a regime with demonstrably greater dependence on heat flux, and finally a regime in which the heat transfer coefficient maximizes and then decreases. At the highest mass flux, the peak heat transfer coefficient was not achieved but it this was due to a limitation in the experimental ability to achieve the peak heat flux due to the elevated pressure drop. Figure 8 shows the unit thermal resistance which is the inverse of the apparent heat transfer coefficient and as expected the data demonstrate that the thermal resistance reaches a minimum at a heat flux that is dependent on the mass flux.

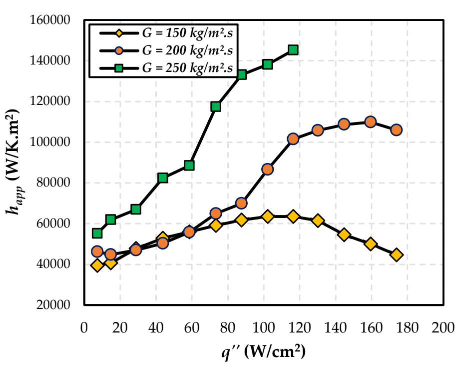

Figure 7: Heat transfer coefficient as a function of heat flux and mass flux

The data of Figures 7 and 8 strongly suggest that vapor quality plays a dominant role in establishing the rates of heat transfer and the pressure drop, just as it does in flow boiling in small channels. The vapor quality is determined by the level of heat flux and mass flow rate as seen in Equations 6 and 7. At a local pore level in the foam, the pore-level heat transfer coefficient is dependent on the local vapor content as well as the local advective flow, i.e., by the mass flux and velocities.

Figures 9 and 10 demonstrate the dependence of apparent heat transfer coefficient and pressure drop on exit vapor quality. The vapor quality of the exiting flow is a measure of the maximum flow quality achieved for a given heat flux and mass flux. Comparison of the data for mass fluxes of 150 and 200 kg/m^{2}s demonstrate that the apparent heat transfer coefficient for each case maximizes at a vapor quality of about 70% beyond which it decreases. A similar behavior is commonly observed in the behavior of heated channels such as in microchannel evaporators and is attributed to a decrease in the local mass flux due to the low-density vapor content as well as to the decrease in the local bulk thermal fluid thermal conductivity again as a result of the increase in low thermal conductivity vapor.

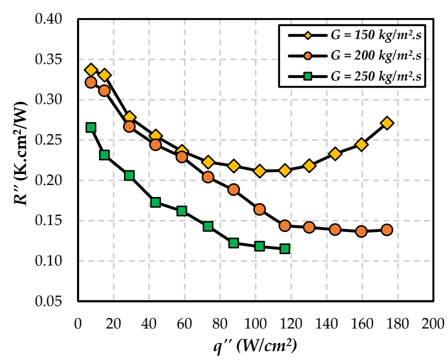

Figure 8: Unit Thermal resistance as a function of heat flux and mass flux

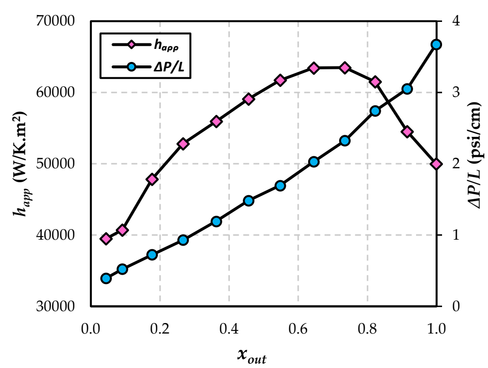

Figure 9: Heat transfer coefficient and pressure drop as a function of exit vapor quality at G = 150 kg/m^{2}s

Commented [MZ1]: It would make more sense to plot the two heat fluxes on the same plot, and the two pressure drop curves on another. Actually why not plot all 3 (since you have data for 3 flow rates)? I think these vapor quality plots are some of the most illuminating of the entire paper, and it would be useful to put all 3 flows in context with respect to one anther.

Commented [DK2R1]: I had a discussion with Carol today morning, and it may not be possible to merge the two exit vapor quality plots because they are separate specific cases and combining them is convoluted. In addition, we decided to include only exit quality plots of 150 and 200 kg/m2s because we don't have complete data for 250 kg/m2s. I will take more data for 250 kg/m2s, up to higher heat fluxes and we will may be include it later after first draft paper acceptance.

Commented [DK3R1]:

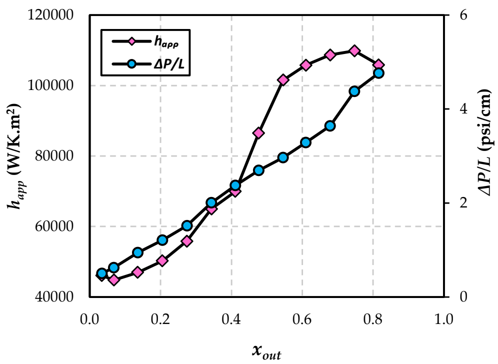

Figure 10: Heat transfer coefficient and pressure drop as a function of exit vapor quality at G = 200 kg/m2s

3.2.3 Pressure drop

For flow boiling in compressed 4X metal foam at a fixed mass flux, the pressure drop as illustrated in Figure 11 increases linearly with increasing heat flux at all mass fluxes. This can be attributed to the increased acceleration of vapor as vapor quality increases at increasing heat fluxes. Figures 9 and 10 alternatively show that pressure drop increases linearly with exit vapor quality. The pressure drop is highly dependent on mass flux, which may be due to increasing frictional losses associated with increasing velocities. Similar observations were reported for two-phase flow boiling in microchannels [4], [5], [10].

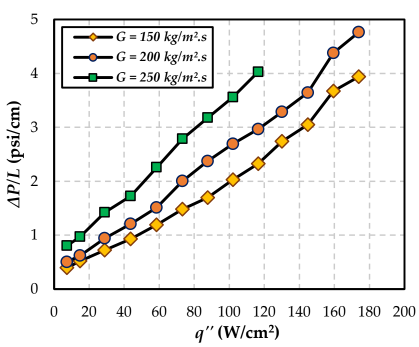

Figure 11: Pressure drop in 4X foam as a function of heat flux and mass flux

4. CONCLUSIONS

Experiments were performed to investigate two-phase flow boiling in compressed metal foams using R134a as the working fluid. The following conclusions can be made from this initial investigation:

1. Compressing the copper metal foam by 4X enhanced thermal performance by up to 300% with proportional increase in pressure drop compared to uncompressed foam
2. Heat fluxes up to 174 W/cm^2 were achieved in the compressed foam at mass fluxes up to 200 kg/m^{2}s with wall superheat less than 40 ºC. The trends at higher mass fluxes indicate that even higher heat fluxes can be achieved
3. No evidence of dryout was observed at heat fluxes up to 174 W/cm^2 at a moderate mass flux of 200 kg/m^{2}s
4. The apparent heat transfer coefficients for the compressed foam increased with increasing mass flux and heat flux. It was found that the heat transfer coefficients for all mass fluxes reached a maximum at an exit vapor quality of about 70%
5. Similarly, the thermal resistance decreased with increasing mass flux and increasing heat flux, reaching a minimum at an exit vapor quality of about 70%
6. Pressure drop increased with increasing mass flux. At all mass fluxes, pressure drop increased linearly with increasing heat flux and exit vapor quality
7. No dynamic instabilities were detected in the ranges of mass flux and heat flux tested
8. By comparing the observed trends in the foam with the data and trends observed for flow boiling in microchannels, it is believed that nucleate boiling may be the dominant phenomena at low mass fluxes and convective boiling at high mass fluxes. Trends were also observed that indicate that thin film evaporation may be an important physical mechanism at the pore level.

ACKNOWLEDGEMENTS

This work was supported by the National Science Foundation Industry/University Collaborative Research Center (NSF I/UCRC) under Grant No. IIP-1738782. Any opinions, findings, and conclusions or recommendations expressed in this article are solely the responsibility of the authors and do not necessarily represent the official views of the NSF. ERG Aerospace Corporation provided the metallic foam samples for experimental testing and designed and fabricated the test section.

REFERENCES

[1] B. Madani, L. Tadrist, and F. Topin, "Experimental analysis of upward flow boiling heat transfer in a channel provided with copper metallic foam," *Applied Thermal Engineering*, vol. 52, no. 2, pp. 336–344, Apr. 2013, doi: 10.1016/j.applthermaleng.2012.11.046.

[2] D. Kisitu and A. Ortega, "Thermal-Hydraulic Analytical Models of Split-Flow Microchannel Liquid-Cooled Cold Plates With Flow Impingement," presented at the ASME

2021 International Technical Conference and Exhibition on Packaging and Integration of Electronic and Photonic Microsystems, Nov. 2021. doi: 10.1115/IPACK2021-73283.

[3] J. B. Marcinichen, J. R. Thome, and B. Michel, “Cooling of microprocessors with micro-evaporation: A novel two-phase cooling cycle,” *International Journal of Refrigeration*, vol. 33, no. 7, pp. 1264–1276, Nov. 2010, doi: 10.1016/j.ijrefrig.2010.06.008.

[4] S. Szczukiewicz, N. Borhani, and J. R. Thome, “Fine-resolution two-phase flow heat transfer coefficient measurements of refrigerants in multi-microchannel evaporators,” *International Journal of Heat and Mass Transfer*, vol. 67, pp. 913–929, Dec. 2013, doi: 10.1016/j.ijheatmasstransfer.2013.08.078.

[5] F. A. Valenzuela Gaete, “An Investigation of the Design and Performance of Two-Phase Cooling Systems for Data Center Electronic Systems,” Ph.D., Villanova University, United States -- Pennsylvania. Accessed: Apr. 24, 2022. [Online]. Available: https://www.proquest.com/docview/2488278548/abstract/E5C4D7817A1341C0PQ/1

[6] “Heat Transfer and Fluid Flow in Minichannels and Microchannels - 2nd Edition.” https://www.elsevier.com/books/heat-transfer-and-fluid-flow-in-minichannels-and-microchannels/kandlikar/978-0-08-098346-2 (accessed Apr. 28, 2022).

[7] D. Kisitu, “Approximate Compact Thermal-Hydraulic Analytical Models for Laminar Microchannel Impingement Liquid-Cooled Cold Plates for Data Center Thermal Management,” M.S.M., Villanova University, United States -- Pennsylvania, 2021. Accessed: Jan. 23, 2022. [Online]. Available: https://www.proquest.com/docview/2618222739/abstract/BE55CBB70F14CD4PQ/1

[8] A. Diani, S. Mancin, L. Doretti, and L. Rossetto, “Low-GWP refrigerants flow boiling heat transfer in a 5 PPI copper foam,” *International Journal of Multiphase Flow*, vol. 76, pp. 111–121, Nov. 2015, doi: 10.1016/j.ijmultiphaseflow.2015.07.003.

[9] “Copper Foam | Duocel® Open Cell Foam Foam,” *https://ergaerospace.com/*. https://ergaerospace.com/copper-foam/ (accessed Apr. 25, 2022).

[10] T. Harirchian and S. V. Garimella, “Boiling Heat Transfer and Flow Regimes in Microchannels—A Comprehensive Understanding,” *Journal of Electronic Packaging*, vol. 133, no. 1, Mar. 2011, doi: 10.1115/1.4002721.

[11] D. W. Kim, A. Bar-Cohen, and B. Han, “Forced convection and flow boiling of a dielectric liquid in a foam-filled channel,” in *2008 11th Intersociety Conference on Thermal and Thermomechanical Phenomena in Electronic Systems*, May 2008, pp. 86–94. doi: 10.1109/ITHERM.2008.4544258.

[12] I. Pranoto and K. C. Leong, “An experimental study of flow boiling heat transfer from porous foam structures in a channel,” *Applied Thermal Engineering*, vol. 70, no. 1, pp. 100–114, Sep. 2014, doi: 10.1016/j.applthermaleng.2014.04.027.

[13] K. K. Wong and K. C. Leong, “Nucleate flow boiling enhancement on engineered three-dimensional porous metallic structures in FC-72,” *Applied Thermal Engineering*, vol. 159, p. -113846, Aug. 2019, doi: 10.1016/j.applthermaleng.2019.113846.

[14] K. E. Gungor and R. H. S. Winterton, “SIMPLIFIED GENERAL CORRELATION FOR SATURATED FLOW BOILING AND COMPARISONS OF CORRELATIONS WITH DATA.,” *Chemical Engineering Research and Design*, vol. 65, no. 2, pp. 148–156, 1987.

[15] S. Mancin, A. Diani, L. Doretti, and L. Rossetto, “R134a and R1234ze(E) liquid and flow boiling heat transfer in a high porosity copper foam,” *International Journal of Heat and Mass Transfer*, vol. 74, pp. 77–87, Jul. 2014, doi: 10.1016/j.ijheatmasstransfer.2014.02.070.

[16] S. G. Kandlikar, “Heat Transfer Mechanisms During Flow Boiling in Microchannels,” *Journal of Heat Transfer*, vol. 126, no. 1, pp. 8–16, Mar. 2004, doi: 10.1115/1.1643090.

[17] S. Krishnan, J. Y. Murthy, and S. V. Garimella, “Direct Simulation of Transport in Open-Cell Metal Foam,” *Journal of Heat Transfer*, vol. 128, no. 8, pp. 793–799, Jan. 2006, doi: 10.1115/1.2227038.

[18] B. Ozmat, B. Leyda, and B. Benson, “Thermal Applications of Open-Cell Metal Foams,” *Materials and Manufacturing Processes*, vol. 19, no. 5, pp. 839–862, Oct. 2004, doi: 10.1081/AMP-200030568.

[19] I. H. Bell, J. Wronski, S. Quoilin, and V. Lemort, “Pure and Pseudo-pure Fluid Thermophysical Property Evaluation and the Open-Source Thermophysical Property Library CoolProp,” *Ind. Eng. Chem. Res.*, vol. 53, no. 6, pp. 2498–2508, Feb. 2014, doi: 10.1021/ie4033999.

